commensurate with L_G. This effect is seen by the strong dependence of DIBL on T_{OX}, thus demonstrating the need for T_{OX} scaling and high-κ (dielectric constant) 2D dielectrics to further enhance the device performance.

The effect of MoS_2 thickness on the device characteristics was systematically explored. At the scaling limit of the gate length, the semiconductor channel thickness must also be scaled down aggressively, as described earlier. The electrostatic control of the SWCNT gate on the MoS_2 channel decreased with increasing distance from the ZrO_2-MoS_2 interface. Thus, as the MoS_2 flake thickness was increased, the channel could not be completely depleted by applying a negative V_{GS}. Because of this effect, the SS for a 12-nm-thick MoS_2 device (~170 mV per decade) was much larger than that of bilayer MoS_2 (~65 mV per decade), and as the thickness of MoS_2 was increased to ~31 nm, the device could no longer be turned off (Fig. 4A). The experimental SS as a function of MoS_2 thickness was qualitatively consistent with the TCAD simulations (Fig. 4B and S10), showing an increasing trend with increasing channel thickness. The unwanted variations in device performance caused by channel thickness fluctuations (Fig. 4B and fig. S10), and the need for low Off state current at short channel lengths (Figs. 1 and 3), thus justify the need for layered semiconductors like TMDs at the scaling limit.

TMDs offer the ultimate scaling of thickness with atomic-level control, and the 1D2D-FET structure enables the study of their physics and electrostatics at short channel lengths by using the natural dimensions of a SWCNT, removing the need for any lithography or patterning processes that are challenging at these scale lengths. However, large-scale processing and manufacturing of TMD devices down to such small gate lengths are existing challenges requiring future innovations. For instance, research on developing process-stable, low-resistance ohmic contacts to TMDs, and scaling of the gate dielectric by using high-κ 2D insulators is essential to further enhance device performance. Wafer-scale growth of high-quality films (*30*) is another challenge toward achieving very-large-scale integration of TMDs in integrated circuits. Finally, fabrication of electrodes at such small scale lengths over large areas requires considerable advances in lithographic techniques. Nevertheless, the work here provides new insight into the ultimate scaling of gate lengths for a FET by surpassing the 5-nm limit (*3*–*7*) often associated with Si technology.

REFERENCES AND NOTES

1. T. N. Theis, P. M. Solomon, *Science* **327**, 1600–1601 (2010).
2. R. Chau, B. Doyle, S. Datta, J. Kavalieros, K. Zhang, *Nat. Mater.* **6**, 810–812 (2007).
3. A. D. Franklin, *Science* **349**, aab2750 (2015).
4. M. Lundstrom, *Science* **299**, 210–211 (2003).
5. M. Luisier, M. Lundstrom, D. A. Antoniadis, J. Bokor, in *Electron Devices Meeting (IEDM), 2011 IEEE International* (IEEE, 2011), pp. 11.12.11–1.12.14.
6. H. Kawaura, T. Sakamoto, T. Baba, *Appl. Phys. Lett.* **76**, 3810–3812 (2000).
7. W. S. Cho, K. Roy, *IEEE Electron Device Lett.* **36**, 427–429 (2015).
8. B. Radisavljevic, A. Radenovic, J. Brivio, V. Giacometti, A. Kis, *Nat. Nanotechnol.* **6**, 147–150 (2011).
9. D. Sarkar *et al.*, *Nature* **526**, 91–95 (2015).
10. H. Liu, A. T. Neal, P. D. Ye, *ACS Nano* **6**, 8563–8569 (2012).
11. H. Wang *et al.*, *Nano Lett.* **12**, 4674–4680 (2012).
12. K. F. Mak, K. L. McGill, J. Park, P. L. McEuen, *Science* **344**, 1489–1492 (2014).
13. D. Jariwala, V. K. Sangwan, L. J. Lauhon, T. J. Marks, M. C. Hersam, *ACS Nano* **8**, 1102–1120 (2014).
14. H. Fang *et al.*, *Proc. Natl. Acad. Sci. U.S.A.* **111**, 6198–6202 (2014).
15. K. S. Novoselov *et al.*, *Proc. Natl. Acad. Sci. U.S.A.* **102**, 10451–10453 (2005).
16. C.-H. Lee *et al.*, *Nat. Nanotechnol.* **9**, 676–681 (2014).
17. Y. Yoon, K. Ganapathi, S. Salahuddin, *Nano Lett.* **11**, 3768–3773 (2011).
18. L. Liu, Y. Lu, J. Guo, *IEEE Trans. Electron. Dev.* **60**, 4133–4139 (2013).
19. D. Wickramaratne, F. Zahid, R. K. Lake, *J. Chem. Phys.* **140**, 124710 (2014).
20. Supplementary materials are available on *Science* Online.
21. K. Suzuki, T. Tanaka, Y. Tosaka, H. Horie, Y. Arimoto, *IEEE Trans. Electron. Dev.* **40**, 2326–2329 (1993).
22. J. Svensson *et al.*, *Nanotechnology* **19**, 325201 (2008).
23. N. Patil *et al.*, *IEEE Trans. NanoTechnol.* **8**, 498–504 (2009).
24. J.-P. Colinge *et al.*, *Nat. Nanotechnol.* **5**, 225–229 (2010).
25. A. Javey *et al.*, *Nano Lett.* **4**, 1319–1322 (2004).
26. X. Zou *et al.*, *Adv. Mater.* **26**, 6255–6261 (2014).
27. Y. Taur, *IEEE Trans. Electron. Dev.* **47**, 160–170 (2000).
28. L. Barbut, F. Jazaeri, D. Bouvet, J.-M. Sallese, *Int. J. Microelectron. Comput. Sci.* **4**, 103–109 (2013).
29. S. Hong, K. Lee, *IEEE Trans. Electron. Dev.* **42**, 1461–1466 (1995).
30. K. Kang *et al.*, *Nature* **520**, 656–660 (2015).

ACKNOWLEDGMENTS

S.B.D. and A.J. were supported by the Electronics Materials program funded by the Director, Office of Science, Office of Basic Energy Sciences, Materials Sciences and Engineering Division of the U.S. Department of Energy under contract DE-AC02-05CH11231. A.B.S. was funded by Applied Materials, Inc., and Entegris, Inc., under the I-RiCE program. J.P.L. and J.B. were supported in part by the Office of Naval Research BRC program. J.P.L. acknowledges a Berkeley Fellowship for Graduate Studies and the NSF Graduate Fellowship Program. Q.W. and M.J.K. were supported by the NRI SWAN Center and Chinese Academy of Sciences President's International Fellowship Initiative (2015VTA031). G.P. and H.-S.P.W. were supported in part by the SONIC Research Center, one of six centers supported by the STARnet phase of the Focus Center Research Program (FCRP) a Semiconductor Research Corporation program sponsored by MARCO and DARPA. A.J., H.-S.P.W., and J.B. acknowledge the NSF Center for Energy Efficient Electronics Science (E^3S). A.J. acknowledges support from Samsung. The authors acknowledge the Molecular Foundry, Lawrence Berkeley National Laboratory for access to the scanning electron microscope. The authors acknowledge H. Fahad for useful discussions about the analytical modeling. All data are reported in the main text and supplementary materials.

SUPPLEMENTARY MATERIALS

www.sciencemag.org/content/354/6308/99/suppl/DC1
Materials and Methods
Supplementary Text
Figs. S1 to S10
Table S1
References (*31*–*44*)

30 June 2016; accepted 7 September 2016
10.1126/science.aah4698

BIOCATALYSIS

An artificial metalloenzyme with the kinetics of native enzymes

P. Dydio,[1,2]* H. M. Key,[1,2]* A. Nazarenko,[1] J. Y.-E. Rha,[1] V. Seyedkazemi,[1] D. S. Clark,[3,4] J. F. Hartwig[1,2]†

Natural enzymes contain highly evolved active sites that lead to fast rates and high selectivities. Although artificial metalloenzymes have been developed that catalyze abiological transformations with high stereoselectivity, the activities of these artificial enzymes are much lower than those of natural enzymes. Here, we report a reconstituted artificial metalloenzyme containing an iridium porphyrin that exhibits kinetic parameters similar to those of natural enzymes. In particular, variants of the P450 enzyme CYP119 containing iridium in place of iron catalyze insertions of carbenes into C–H bonds with up to 98% enantiomeric excess, 35,000 turnovers, and 2550 hours^{-1} turnover frequency. This activity leads to intramolecular carbene insertions into unactivated C–H bonds and intermolecular carbene insertions into C–H bonds. These results lift the restrictions on merging chemical catalysis and biocatalysis to create highly active, productive, and selective metalloenzymes for abiological reactions.

The catalytic activity of a metalloenzyme is determined by both the primary coordination sphere of the metal and the surrounding protein scaffold. In some cases, laboratory evolution has been used to develop variants of native metalloenzymes for selective reactions of unnatural substrates (*1*, *2*). Yet with few exceptions (*3*), the classes of reactions that such enzymes undergo are limited to those of biological transformations. To combine the favorable qualities of enzymes with the diverse reactivity of synthetic transition-metal catalysts, abiological transition-metal centers or cofactors have been incorporated into native proteins. The resulting artificial metalloenzymes catalyze classes of reactions for which there is no known enzyme (abiological transformations) (*3*, *4*).

Although the reactivity of these artificial systems is new for an enzyme, the rates of these reactions have been much slower and the

[1]Department of Chemistry, University of California, Berkeley, CA 94720, USA. [2]Chemical Sciences Division, Lawrence Berkeley National Laboratory, 1 Cyclotron Road, Berkeley, CA 94720, USA. [3]Department of Chemical and Biomolecular Engineering, University of California, Berkeley, CA 94720, USA. [4]Molecular Biophysics and Integrated Bioimaging Division, Lawrence Berkeley National Laboratory, 1 Cyclotron Road, Berkeley, CA 94720, USA.
*These authors contributed equally to this work. **†Corresponding author. Email: jhartwig@berkeley.edu**

turnover number (TON) much lower than those of reactions catalyzed by free metal complexes in organic solvents and lower than those typical of natural enzymes (*4*, *5*). In addition to lacking high activity, these enzymes lack practical characteristics of enzymes for synthetic applications, such as suitability for preparative-scale reactions and potential to be recovered and reused (*6*). One reason that artificial metalloenzymes react more slowly than native enzymes is the absence of a defined binding site for the substrate. Natural enzymes generally bind their substrates with high affinity and in a conformation that leads to extremely fast rates and high selectivity (*7*). If the artificial metalloenzyme is generated by incorporating a full metal-ligand complex into the substrate-binding site of a natural enzyme or protein, the space remaining to bind a reactant for a catalytic process is limited, and the interactions by which the protein binds the reactant are compromised (*4*, *8*). Recently, we reported artificial metalloenzymes generated by the formal replacement of an abiological metal for the natural iron in myoglobin that catalyzes abiological reactions (*9*), but the activity of the resulting enzymes was far from that needed for synthetic applications (*6*). Here, we show that artificial metalloenzymes created by substituting an iridium-methyl unit for the iron in cytochrome P450 enzymes (*10*) and modified by means of laboratory evolution catalyze abiological reactions with activities that are comparable with those of native enzymes (*5*).

P450 enzymes constitute a superfamily of heme-binding monooxygenases that are involved in various biosynthetic pathways, catalyzing reactions that encompass chemo-, regio-, stereo-, and site-selective C–H hydroxylations of complex natural products (*11*). We hypothesized that artificial metalloenzymes that are created with P450s from thermophiles, such as CYP119 (*12*) from *Sulfolobus solfataricus*, could improve the thermal stability of the resulting artificial metalloenzyme and create the potential to conduct reactions at elevated temperatures. Studies on stability revealed that the Ir(Me)-PIX protein formed from CYP119 did have a much higher melting temperature (T_m = 69°C) than those formed from the more commonly used P450-BM3 (45°C) or P450-CAM (40°C). Therefore, this protein was used for our studies on catalytic reactions.

By studying the model reaction to convert diazoester **1** into dihydrobenzofuran **2**, which does not occur in the presence of natural Fe-PIX enzymes, we found that the activity and selectivity of Ir(Me)-PIX CYP119 enzymes are readily evolved through molecular evolution of the natural substrate-binding site of the CYP119 scaffold (Figs. 1 and 2). The wild type (WT) Ir(Me)-CYP119 enzyme and its variant C317G [bearing a mutation that introduces space to accommodate the axial ligand of the Ir(Me)-PIX cofactor] (*13*) catalyze the intramolecular carbene insertion into a C–H bond to form **2**, although with low rates [turnover frequency (TOF) = 0.23 and 0.13 min^{-1}, respectively] and enantioselectivities (ee = 0 and 14%, respectively) for reactions conducted with 5 mM **1** and 0.1 mole % (mol %) catalyst. (Single-letter abbreviations for the amino acid residues are as follows: A, Ala; C, Cys; D, Asp; E, Glu; F, Phe; G, Gly; H, His; I, Ile; K, Lys; L, Leu; M, Met; N, Asn; P, Pro; Q, Gln; R, Arg; S, Ser; T, Thr; V, Val; W, Trp; and Y, Tyr. In the mutants, amino acids were substituted at specific locations; for example, C317G indicates that cysteine at position 317 was replaced by glycine.) To identify mutants that form **2** with higher rates and enantioselectivity, we used a directed evolution strategy targeting the residues close to the active site (L69, A209, T213, and V254) (Fig. 2). To retain the hydrophobicity of the active site, we introduced only hydrophobic and uncharged residues (V, A, G, F, Y, S, and T) through site-directed mutagenesis within a library of 24 double mutants of CYP119. The mutant C317G, T213G formed **2** with 68% ee and 80-fold higher activity (TOF = 9.3 min^{-1}) than did that of the single mutant C317G under the same reaction conditions, described previously. Two additional rounds of evolution, in which ~150 additional variants were analyzed, led to the quadruple mutant C317G, T213G, L69V, V254L (hereafter referred to as CYP119-Max), which formed **2** with 94% ee and with an initial TOF of 43 min^{-1}. This rate is more than 180 times faster than that of the WT variant.

Kinetic studies provided insight into the origin of the differences in the enzymatic activity between the various mutants of Ir(Me)-CYP119. In particular, we determined the standard Michaelis-Menten kinetic parameters (k_{cat} and K_M) for the mutants at each stage of the evolution. Using these parameters, we determined the catalytic efficiency of each enzyme, which is defined as k_{cat}/K_M (*14*) and considered to be one of the most relevant parameters for comparing engineered enzymes to natural enzymes (*5*). The affinity of substrate **1** for the WT enzyme is weak, as revealed by a high K_M (> 5 mM). The single mutant C317G, which lacks a sidechain at this position that could act as an axial ligand, exhibits higher substrate affinity (K_M = 3.1 mM), catalytic activity (k_{cat} = 0.22 min^{-1}), and therefore overall enzyme efficiency (k_{cat}/K_M = 0.071 min^{-1} mM^{-1}) than that of the WT enzyme. The double mutant T213G, C317G of Ir(Me)-CYP119 reacts with Michaelis-Menten parameters (k_{cat} = 4.8 min^{-1} and K_M = 0.40 mM, k_{cat}/K_M = 12 min^{-1} mM^{-1}) that are far more favorable than those of the single mutant C317G. The incorporation of two additional mutations (L69V, V254L) led to further improvements of both k_{cat} and K_M, creating an enzyme (CYP119-Max) with an efficiency that is greater than 4000 times (k_{cat} = 45.8 min^{-1}, K_M = 0.17 mM, and k_{cat}/K_M = 269 min^{-1} mM^{-1}) that of the WT system. These kinetic parameters mark a vast improvement over those of the variant of myoglobin Ir(Me)-PIX-mOCR-Myo H93A, H64V (k_{cat} = 0.73 min^{-1}, K_M = 1.1 mM, and k_{cat}/K_M = 0.66 $min^{-1}mM^{-1}$) (Fig. 2) (*15*). Furthermore, the rates of reactions catalyzed by CYP119-Max at concentrations below K_M are more than 20 times higher than those catalyzed by the free iridium-porphyrin in the presence of the same substrate concentration (TOF = 21 min^{-1} versus TOF = 0.93 min^{-1} at 0.15 mM **1**, respectively), even though the free cofactor lacks any steric encumbrance near the metal site necessary to enable selective catalysis. These results show the value of conducting this iridium-catalyzed reaction within the enzyme active site to control selectivity and increase the reaction rate simultaneously.

The kinetic parameters of reactions catalyzed by the Ir(Me)-PIX CYP119-Max enzyme are comparable with those of native reactions catalyzed by the natural enzymes involved in intermediate

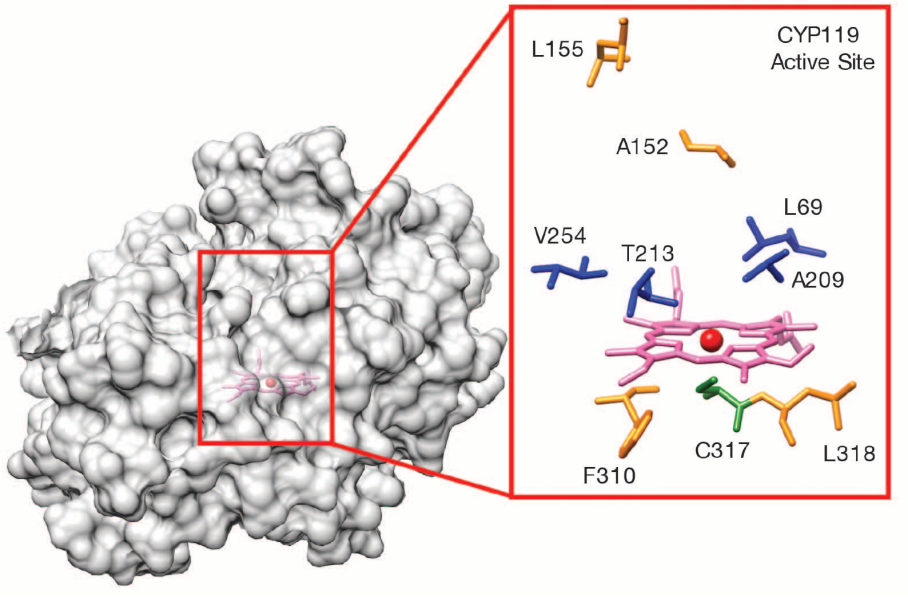

Fig. 1. Structure of WT Fe-CYP119. Image was prepared in Chimera from Protein Data Bank 1IO7. (**Left**) Complete structure of Fe-CYP119. (**Right**) Active-site residues modified during directed evolution of the protein scaffold to increase activity and selectivity for carbene insertions into C–H bonds.

and secondary metabolism (*5*), such as many cytochromes P450 (*16*). The binding affinity of Ir(Me)-CYP119-Max for the abiological substrate **1** is even higher than the affinity of P450s for their native substrates (compare K_M = 0.17 mM for CYP119-Max with K_M = 0.298 mM for P450-BM3 and its native substrate lauric acid) (*17*) and similar to the median K_M value for natural enzymes of this class (0.13 mM) (*5*). In addition, the k_{cat} of 45.8 min^{-1} for this enzyme is within an order of magnitude of the median k_{cat} of natural enzymes responsible for the production of biosynthetic intermediates (312 min^{-1}) and secondary metabolites (150 min^{-1}) (*5*).

The potential to evolve proteins having advantageous enzyme-substrate interactions should also create the possibility to catalyze the insertion of carbenes into the C–H bonds of diverse and less reactive substrates (Fig. 3). Directed evolution targeting high stereoselectivity led to mutants that form products **3** to **7** in up to ±98% ee, in reactions conducted with a fixed catalyst loading (0.17 mol %). The reactions to form products **3** to **5** show that the enzyme reacts as selectively with substrates containing substituents on the aryl ring as it does for unsubstituted **2**. Such reactivity is relevant to contemporary synthetic challenges. For example, compound (***S***)-**5** is an intermediate in the synthesis of BRL *37959*—a potent analgesic—and was prepared previously by means of kinetic resolution (*18*). This product was formed by variant 69Y-152W-213G in 94% ee. Product **6** results from carbene insertion into a secondary C–H bond, and product **7** results from carbene insertion into a sterically hindered, secondary C–H bond. Directed evolution furnished a mutant capable of forming **7** with high enantio- and diastereoselectivity (dr) favoring the cis isomer [90% ee, 12:1 dr (cis:trans)]. The previously reported Ir(Me)-PIX enzymes based on myoglobin produced this product in only trace amounts, and the free Ir(Me)-PIX cofactor formed predominantly the trans isomer (3:1 dr, trans:cis). This reversal of diastereoselectivity from that of the free Ir(Me)-PIX cofactor to that of the artificial metalloenzyme highlights the ability of strong substrate-enzyme interactions to override the inherent selectivity of a metal cofactor or substrate.

Ir(Me)-CYP119-Max also catalyzes the insertion of carbenes into fully unactivated C–H bonds. Although the structure of substrate **7** in Fig. 4 appears similar to that of substrate **1**, the primary C–H bonds in **7** are stronger and less reactive than those in **1**, which are located alpha to an oxygen atom (*19*).

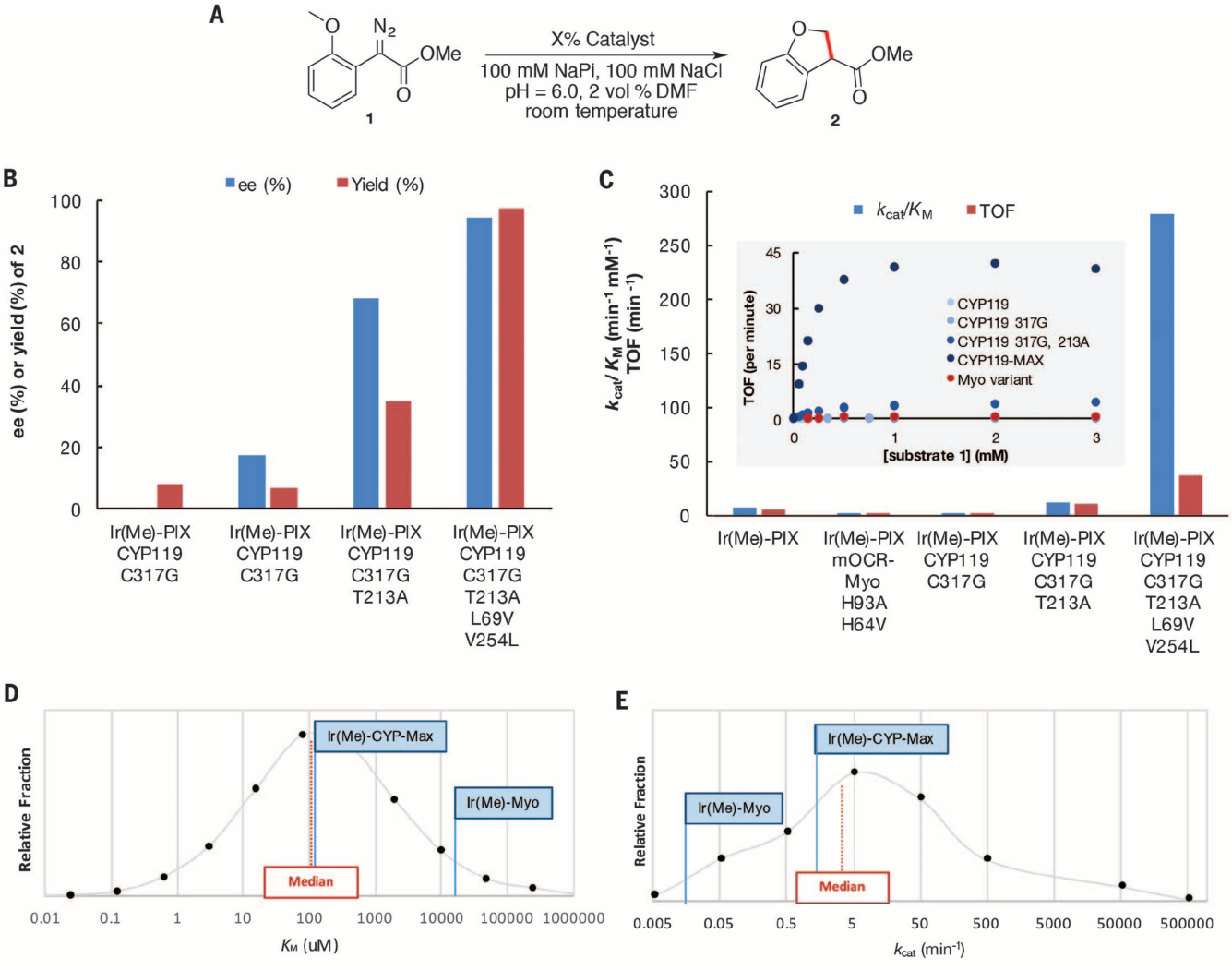

Fig. 2. Directed evolution of Ir(Me)-PIX CYP119 for enantioselective insertions of carbenes into C–H bonds. (**A**) Model reaction converting diazoester **1** to dihydrobenzofuran **2**. (**B**) Enantioselectivity and yields for the formation of **2** catalyzed by evolved variants of CYP119 (0.17% catalyst loading, 10 mM substrate). (**C**) Kinetic parameters describing the formation of **2** by variants of CYP119 (0.1 mol % catalyst loading, 5 mM substrate). For free Ir(Me)-PIX, k_1 (the first-order kinetic constant) is listed instead of k_{cat}/K_M (*16*). (Inset) Dependence of TOF on the initial concentration of **1** for reactions using 0.005 mM catalyst. (**D** and **E**) Comparison of K_M and k_{cat} values for CYP119-Max with those of natural enzymes involved in the metabolism of intermediate and secondary metabolites (*5*); for comparison, the kinetic parameters for Ir(Me)-PIX mOCR-myoglobin (H93A and H64V) catalyzing the same transformation are shown.

In fact, there are no metal catalysts of any type reported to form indanes via carbene insertion into an unactivated C–H bond with synthetically useful enantioselectivities. The synthesis of such chiral moieties was achieved only in a diastereoselective fashion, when a stoichiometric amount of a chiral auxiliary was built into the substrate (*20*). In contrast, Ir(Me)-CYP119-Max catalyzed the formation of **8** in 90% ee, with no need for the auxiliary. To observe substantial amounts of this product (TON = 31), the reaction was conducted at 40°C; the enantioselectivity of the product at this temperature was the same as that of the small quantity of product formed at room temperature.

In addition to catalyzing intramolecular reactions with unactivated C–H bonds, Ir(Me)-CYP119-Max catalyzes intermolecular carbene insertion into a C–H bond. This reaction is challenging because the metal-carbene intermediate can undergo competitive diazo coupling or insert the carbene unit into the O–H bond of water (*21*, *22*). In fact, the model reaction between phthalan (**10**) and ethyl diazoacetate (EDA) forms alkene and alcohol as the dominant products when catalyzed by the

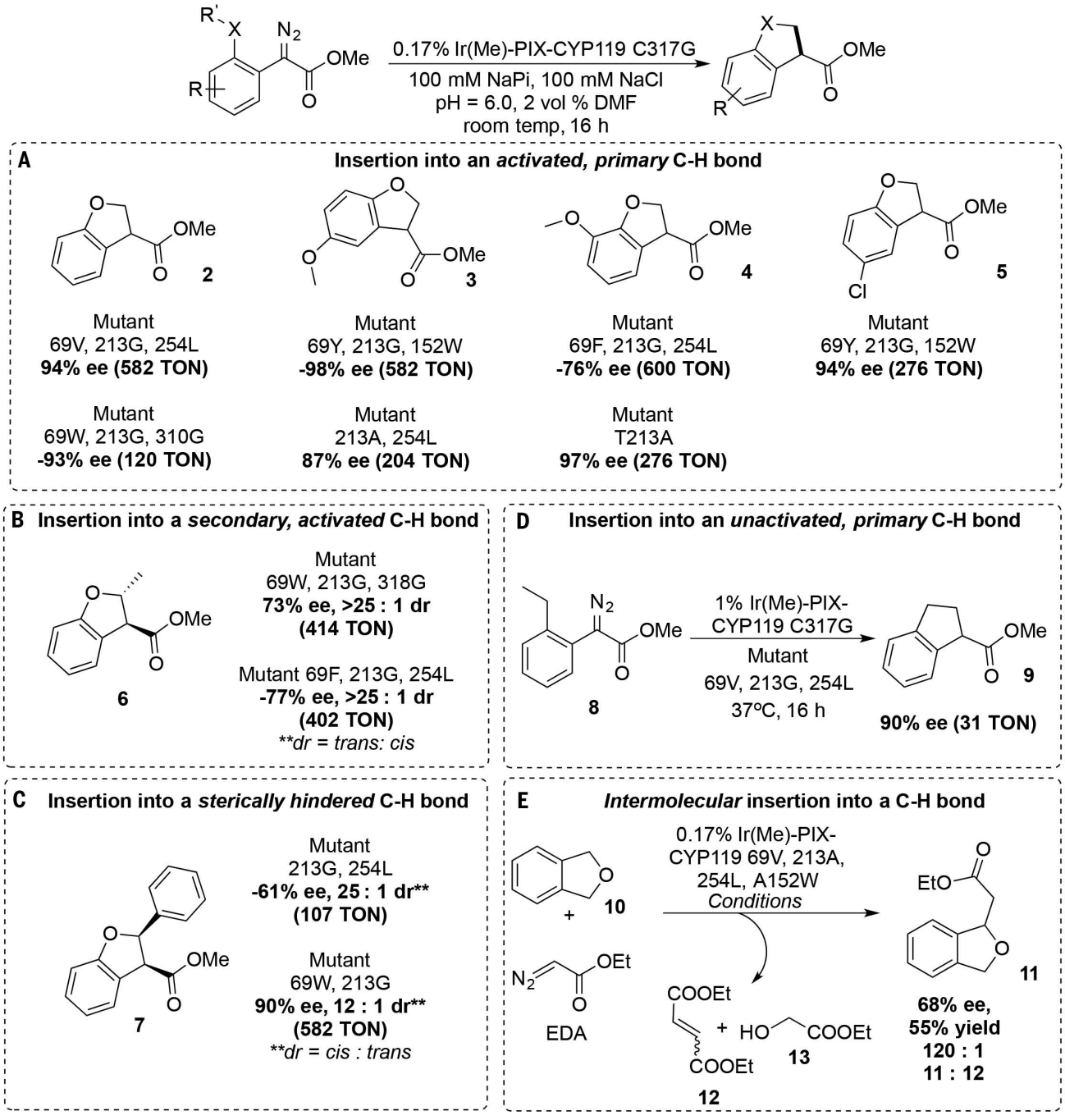

Fig. 3. Selective variants of Ir(Me)-PIX CYP119. These variants catalyze enantioselective intra- and intermolecular C–H carbene insertion reactions of activated and unactivated C–H bonds. (**A** to **D**) Intramolecular C–H carbene insertion reactions. Reactions were conducted at room temperature unless otherwise noted. (**E**) An intermolecular C–H carbene insertion reaction. Conditions: **10** (10 μmol) and EDA (100 μmol). EDA was added as a 50% solution in *N*,*N*′-dimethylformamide over 1 hour by use of a syringe pump.

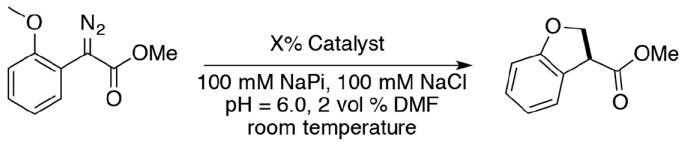

Reactions Conducted at a Range of Scales

mmol/ mg substrate	% catalyst	TON	Yield	ee (%)
0.0025 mmol, 0.5 mg	0.17%	330	56% yield (GC)	94%
0.2 mmol, 40 mg	0.25%	192	48% yield (Isolated)	92%
0.2 mmol, 40 mg	0.05%	1060	53% yield (Isolated)	92%
1.0 mmol, 206 mg	0.017%	3529	60% yield (Isolated)	93%
5.0 mmol, 1 gram	0.017%	3235	55% yield (Isolated)	93%

Reactions Conducted with a Range of Catalyst Loadings

[substrate], mg substrate	[catalyst]	TON	Yield	ee (%)
100 mM, 5 mg	0.025 mM	3800	95% yield	92%
100 mM, 5 mg	0.01 mM	8326	83% yield	92%
100 mM, 10 mg	0.0025 mM	30293	76% yield	92%
200 mM, 10 mg	0.0025 mM	35129	44% yield	91%

Fig. 4. Productivity of Ir(Me)-PIX CYP119. Intramolecular C–H carbene insertion reactions of substrate **1** catalyzed by Ir(Me)-PIX CYP119-Max under synthetically relevant reaction conditions.

free Ir(Me)-PIX cofactor; only trace amounts of carbene insertion product **11** were formed. In sharp contrast, the same reaction catalyzed by the mutant Ir(Me)-PIX CYP119-Max-A152F occurred to form **11** in 55% yield with 330 TON and 68% ee. Dimerization of the carbene when catalyzed by Ir(Me)-CYP119-Max is limited, presumably because of selective binding and preorganization of the substrate; the selectivity for formation of the product from C–H insertion **11** over the alkene side product **12** was 70-fold higher when catalyzed by Ir(Me)-PIX CYP119-Max-A152F than when catalyzed by the free cofactor.

For the ultimate goal of applying artificial metalloenzymes to the synthesis of organic molecules for fine chemicals, the reactions conducted by such catalytic systems should occur on preparative scales with high substrate concentrations, and the enzyme should react with high TONs and be amenable to attachment to a solid support for recycling. We found that a series of reactions containing between 40 mg and 1 g of substrate **1** catalyzed by Ir(Me)-CYP-Max occurred with yields and enantioselectivities that were similar to each other (91 to 94% ee), showing that the outcome of the reaction is independent of the scale (Fig. 4). Moreover, with 200 mM substrate, reactions catalyzed by Ir(Me)-CYP-Max (0.0025 mM) formed product **2** with up to 35,000 TON without loss of enantioselectivity (93% ee) (Fig. 4). Thus, this artificial metalloenzyme operates with high productivity under conditions suitable for preparative scales. Last, Ir(Me)-CYP-Max supported on CNBr-activated sepharose catalyzed the conversion of **1** to **2** via carbene insertion into a C–H bond in 52% yield and 83% ee. This supported catalyst was used, recovered, and recycled four times without loss of the enantioselectivity for formation of **2**, while retaining 64% of the activity (fig. S11).

Enzymes containing abiological transition-metal active sites that exhibit the kinetics, selectivity, and evolutionary potential of natural enzymes have been a major goal of catalyst design. Here, we show that artificial metalloenzymes catalyzing abiological processes can possess the fundamental characteristics of natural enzymes: fast kinetics, high productivity, and high selectivity under the same reaction conditions. Taken together, our results show that the kinetics of artificial metalloenzymes need not limit the merging of chemical and biocatalysis.

REFERENCES AND NOTES

1. M. W. Peters, P. Meinhold, A. Glieder, F. H. Arnold, *J. Am. Chem. Soc.* **125**, 13442–13450 (2003).
2. G.-D. Roiban, R. Agudo, M. T. Reetz, *Angew. Chem. Int. Ed. Engl.* **53**, 8659–8663 (2014).
3. T. K. Hyster, F. H. Arnold, *Isr. J. Chem.* **55**, 14–20 (2015).
4. J. C. Lewis, *ACS Catal.* **3**, 2954–2975 (2013).
5. A. Bar-Even *et al.*, *Biochemistry* **50**, 4402–4410 (2011).
6. K. M. Koeller, C.-H. Wong, *Nature* **409**, 232–240 (2001).
7. D. Ringe, G. A. Petsko, *Science* **320**, 1428–1429 (2008).
8. M. R. Ringenberg, T. R. Ward, *Chem. Commun. (Camb.)* **47**, 8470–8476 (2011).
9. H. M. Key, P. Dydio, D. S. Clark, J. F. Hartwig, *Nature* **534**, 534–537 (2016).
10. Materials and methods are available as supplementary materials on *Science* Online.
11. A. Sigel, H. Sigel, R. K. O. Sigel, Eds., *The Ubiquitous Roles of Cytochrome P450 Proteins* (John Wiley & Sons, 2007).
12. K. S. Rabe, K. Kiko, C. M. Niemeyer, *ChemBioChem* **9**, 420–425 (2008).
13. J. A. McIntosh, T. Heel, A. R. Buller, L. Chio, F. H. Arnold, *J. Am. Chem. Soc.* **137**, 13861–13865 (2015).
14. J. M. Berg, J. L. Tymoczko, L. Stryer, *Biochemistry* (W.H. Freeman, ed. 5, 2002).
15. This variant of myoglobin was used for comparison because this variant forms **2** with both high yield and high enantioselectivity [relative to other mutants of Ir(Me)-PIX Myo].
16. J. Romeo, Ed., *Secondary Metabolism in Model Systems* (Elsevier, 2004).
17. M. A. Noble *et al.*, *Biochem. J.* **339**, 371–379 (1999).
18. P. Bongen, J. Pietruszka, R. C. Simon, *Chemistry* **18**, 11063–11070 (2012).
19. S. M. Paradine, M. C. White, *J. Am. Chem. Soc.* **134**, 2036–2039 (2012).
20. B. Hong *et al.*, *J. Am. Chem. Soc.* **137**, 11946–11949 (2015).
21. P. Srivastava, H. Yang, K. Ellis-Guardiola, J. C. Lewis, *Nat. Commun.* **6**, 7789 (2015).
22. N. M. Weldy *et al.*, *Chem. Sci.* **7**, 3142–3146 (2016).

ACKNOWLEDGMENTS

This work was supported by the Director, Office of Science, of the U.S. Department of Energy under contract DE-AC02-05CH11231; by the NSF (graduate research fellowship to H.M.K.), and the Netherlands Organization for Scientific Research (the Rubicon postdoctoral fellowship 680-50-1306 to P.D.). We thank the QB3 MacroLab facility (competent cells), the University of California, Berkeley DNA Sequencing Facility (plasmid sequencing), and T. Iavarone and the QB3 Mass Spectrometry Facility [nano–electrospray ionization (NS-ESI) mass spectrometry data collection, supported by NIH grant 1S10OD020062-01] for native nanoESI-MS data and analysis. All data are provided in the supplementary materials. J.F.H., H.M.K., P.F.D., and D.S.C. are inventors on U.S. patent application numbers 62/241,487 and 62/384,011, submitted by the Lawrence Berkeley National Laboratory, that covers preparation and application of artificial metalloenzymes containing noble metal-porphyrins.

SUPPLEMENTARY MATERIALS

www.sciencemag.org/content/354/6308/102/suppl/DC1
Materials and Methods
Figs. S1 to S12
Tables S1 to S7
References (*23*–*28*)

28 June 2016; accepted 12 September 2016
10.1126/science.aah4427

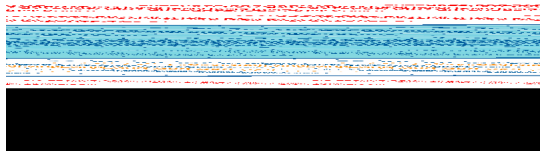

An artificial metalloenzyme with the kinetics of native enzymes
P. Dydio, H. M. Key, A. Nazarenko, J. Y.-E. Rha, V. Seyedkazemi, D. S. Clark and J. F. Hartwig (October 6, 2016)
Science **354** (6308), 102-106. [doi: 10.1126/science.aah4427]

Editor's Summary

Something like the real thing

Artificial metalloenzymes ideally combine the favorable properties of natural enzymes with the high efficiency of synthetic catalysts. Inserting new metal groups into existing native proteins, however, often leads to poorer overall catalytic efficiency. To break through this limitation, Dydio *et al.* replaced the iron in the heme group of cytochrome P450 with iridium and subjected it to directed evolution. The enzyme catalyzed a range of reactions with kinetics similar to those of the native enzyme. It was also able to functionalize fully unactivated C-H bonds, a reaction that previously has only been mediated by synthetic catalysts. Moreover, the artificial enzyme was stable across temperatures and scales that are used industrially.

Science, this issue p. 102